An Idealized Representation of a Stratospheric Aerosol Injection in E3SM - technical implementation description

Joe Hollowed

University of Michigan 2023

Contents

1 Introduction

In what follows, we will be applying an idealized model of stratospheric aerosol injection to the 1991 eruption of the stratovolcano Mt. Pinatubo in western Luzon, Phillipines near 15°N. Particularly relevant to the climate impacts of this eruption (McCormick et al., 1995; Robock, 2000) was the injection of sulfur species into the atmosphere, namely sulfur dioxide (SO_2), and its subsequent reaction product, *sulfate aerosol* (a combination of H_2O and H_2SO_4 (sulfuric acid)). Also present was an enormous amount of ash, ice, and water.

This document describes a method of aerosol injection and radiative forcing that is simple enough to be applied to idealized dry component sets of a coupled climate model which lacks any parameterizations for radiative transfer, aerosol physics and chemistry, or other implementations of volcanic forcings. It has, in particular, been developed assuming a background climate governed by the Held-Suarez-Williamson (HSW) configuration of atmospheric forcing (Held & Suarez, 1994; Williamson et al., 1998). Section 2 describes the aerosol tracer source and sink terms, and total mass burden normalization. Section 3 describes the parameters defining each tracer species, and Sections 3.1 gives the strategy for sulfate formation from SO_2. Sections 3.2.2−3.2.3 give the methods of stratospheric heating and surface cooling by considerations of shortwave and longwave extinction. Section 4 compactly presents the most important equations and a table of model parameters, and finally Section 5 presents an offline single-column version of the model, for which an analytic solution is presented.

2 Injection model

Here we consider a simple model for the mass tendency of a tracer j representing an idealized volcanic stratospheric aerosol injection (SAI) event:

$$\frac{\partial m_j}{\partial t} = R(m_j) + f \tag{1}$$

where $R(m)$ is an exponential removal function with e-folding timescale $1/k_j$,

$$R(m_j) = -k_j m_j \tag{2}$$

and f is a source term which describes the injection of a 3D aerosol mass into the stratosphere

$$f = A_j H(\phi, \lambda) V(z) T(t) \tag{3}$$

with separable horizontal and vertical dependencies $H(\phi, \lambda)$ and $V(z)$. The coordinates ϕ, λ, and z are latitude, longitude, and height, respectively. We take the time dependence to be a simple step function, representing a constant injection beginning at time t_0 and ending at $t_0 + \delta t$, after which the source vanishes,

$$T(t) = \begin{cases} 1 & \text{if } t_0 \leq t \leq t_0 + \delta t \\ 0 & \text{if else} \end{cases} \tag{4}$$

in which case, the mass injection as a function of time is

$$m_j(\phi, \lambda, z, t) = \frac{\partial m_j}{\partial t} \delta t \tag{5}$$

The source function is normalized by the constant A, which scales the *total injected mass* to a known parameter M_j, by

$$M_j = f \delta t = A_j \delta t H(\phi, \lambda) V(z) \tag{6}$$

In deriving A, let us first discretize the functions H and V on columns i and vertical levels k. If instead this constant is derived from the continuous expression, we may lose some of the total mass to numerical diffusion once the mass distribution is deposited onto the model grid. The discretized forms for the mass tendency and total mass are

$$\frac{\partial m_{j,i,k}}{\partial t} = -k_j m_j + A_j H(\phi_i, \lambda_i) V(z_k), \tag{7}$$

$$M_j = \sum_i \sum_k A_j \delta t H(\phi_i, \lambda_i) V(z_k) \tag{8}$$

We will now assume a very simple form for the horizontal dependence H such that the injection occurs uniformly across the horizontal area of a single column i'. If the desired center of the plume is to be at (ϕ_0, λ_0), then i' is chosen to minimize the great circle distance $r(\phi_{i'}, \lambda_{i'})$, where

$$r(\phi, \lambda) = a \cos^{-1} \left[\sin \phi \sin \phi_0 + \cos \phi \cos \phi_0 \cos(|\lambda - \lambda_0|) \right] \tag{9}$$

In the discretized expression, the column selection is achieved by setting H to the Kronecker-Delta function $\delta_{ii'}$ as

$$H(\phi_i, \lambda_i) = \delta_{ii'} \equiv \begin{cases} 1 & \text{if } i = i' \\ 0 & \text{if } i \neq i' \end{cases} \tag{10}$$

2

which collapses the column sum in Eq.(8) and gives the normalization in terms of the vertical mass distribution:

$$M_j = A_j \delta t \delta_{ii'} \sum_k V(z_k) \tag{11}$$

$$\implies A_j = \frac{M_j}{\delta t \sum_k V_k} \tag{12}$$

Here, we have discarded the delta function from the result to avoid a division by zero in the case that $i \neq i'$, justified by the fact that injection is already constrained to vanish under this condition by the presence of H in the tendency $\partial m_j / \partial t$. We have also defined $V_k \equiv V(z_k)$.

Rather than $\partial m_j / \partial t$ itself, the quantity ultimately required by EAM's physics interface is the tendency of the tracer *mixing ratio* $q_j \equiv m_j / m_{\mathrm{atm}}$. Given the derivations above, this is

$$\frac{\partial q_{j,i,k}}{\partial t} = \frac{1}{m_{\mathrm{atm},i,k}} \left[-k_j m_j + \frac{M_j}{\delta t \sum_k V_k} V_k \delta_{ii'} \right] \tag{13}$$

The air mass m_{atm} can be replaced by

$$m_{\mathrm{atm},i,k} = \rho_{i,k} a_i \Delta z_{i,k} \tag{14}$$

where $\rho_{i,k}$ is the air density in this grid cell, a_i is the column area, and $\Delta z_{i,k}$ is the vertical thickness of this grid cell. This is further reduced to a function of nothing but the local pressure thickness $\Delta p_{i,k}$ via the hydrostatic approximation:

$$\frac{\Delta p_{i,k}}{\Delta z_{i,k}} + \rho_{\mathrm{atm},i,k} g = 0 \tag{15}$$

$$\implies \rho_{\mathrm{atm},i,k} \Delta z_{i,k} = \frac{\Delta p_{i,k}}{g} \tag{16}$$

$$\implies m_{\mathrm{atm},i,k} = \frac{\Delta p_{i,k} a_i}{g} \tag{17}$$

(the sign is discarded from the first to second line, since this only communicates that p decreases with z, and what we care abut is the magnitude. Consider it a "flip of integration bounds").

The final expression for the update of tracer j at position (i, k) for $t \in [t_0, t_0 + \delta t]$ is then

$$\frac{\partial q_{j,i,k}}{\partial t} = \frac{g}{\Delta p_{i,k} a_i} \left[-k_j m_j + \frac{M_j}{\delta t \sum_k V_k} V_k \delta_{ii'} \right] \tag{18}$$

For the vertical dependence $V(z)$, we follow Fisher et al. (2019) and assume a Gaussian distribution (which in this case we use as a pmf with units of inverse height) defined by a center of mass altitude μ, and a geometrical standard deviation:

$$V(z) = \exp\left(-\frac{1}{2} \frac{(z - \mu)^2}{(1.5 \ \mathrm{km})^2} \right) \frac{1}{\mathrm{km}} \tag{19}$$

For the deviation, we use 1.5 km, which is a compromise between Fisher et al. (2019) and the vertical width of the parabolic injection profile of Stenchikov et al. (2021). In hydrostatic models

3

(such as E3SM), the height z is a diagnostic quantity. Therefore, the vertical profile needs to be computed at each timestep. Despite this, we choose not to approximate z, and use the per-timestep diagnostic quantity, since it need only be done for the very brief injection duration. All species j are co-injected at the same height and with the same deviation, and we do not include a normalization coefficient in $V(z)$, since A_j is already scaled by $\sum_k V_k$.

As a final note; for the vertical dependence, we initially attempted to adopt $V(z)$ from the parameter ensemble Pinatubo study described in Sheng et al. (2015). There, they assume initial injection profiles of a log-normal form, and generate a large ensemble of injections in a 2D aerosol model with respect to the shape parameters of this distribution. Scoring of the ensemble members was done via a weighted approach which utilized agreement with data in four metrics: (1) SO_2 mixing ratio data from the Microwave Limb Sounder (MLS), (2) the global aerosol burden from the High-resolution Infrared Radiation Sounder (HIRS) and the Stratospheric Aerosol and Gas Experiment (SAGE-4λ), (3) particle number concentration in various size channels from the Optical Particle Counter (OPC), and (4) extinction coefficients from the Stratospheric Aerosol and Gas Experiment (SAGE II). After using the highest-scoring profile result in our simulations, we found that the plume lofts to altitudes that are much too high.

The conclusion here, as articulated by Stenchikov et al. (2021), is that this analysis misses the mechanism by which the plume is delivered to the lower stratosphere. This is by design; Sheng et al. (2015) prescribe the initial mass loading via a zonally-symmetric profile, and the SAGE and HIRS observations that were used in the ensemble scoring missed the actual eruption. In other words, those authors use "initial mass distribution" to mean the mass distribution realized only *after* the plume is rapidly lofted by co-ignimbrite (ash-driven) convection. Because we include the eruption itself in our model, it is suggested that we should instead inject just above the tropical tropopause, near $\mu = $ 17-18 km (Stenchikov et al., 2021; Fisher et al., 2019), and then allow this self-lofting process to carry the plume to a level of neutral buoyancy in the stratosphere, which is expected to be driven by a vertical velocity of $w \approx 1$ km/day with initial heating rates of the dense, fresh volcanic plume around 20 K/day. See Section 3 for details.

3 Tracer constituents and feedback to the atmospheric state

Here we describe the simultaneous injection SO_2, sulfate, and ash tracers. Observations giving the total injected mass and e-folding time for each species were estimated from satellite data and published in Guo et al. (2004a) and Guo et al. (2004b), Barnes and Hofmann (1997). Table 1 gives the parameter values chosen for this work, in which case the model describes the 24-hour injection of a plume centered on 14 km in the vertical, uniformly over a single column. We assume no background values for any of the injected species prior to the eruption, as in some other studies (e.g. Bekki and Pyle (1994)). Figure 5 shows an analytic advection-free solution to the problem (described in Section 5).

In the case that we simply insert choices for M_j and k_j for a given tracer into the framework presented in Section 2, and allow the model to evolve the tracer mixing ratio by the tendencies as defined, they will be advected with the winds, but will otherwise behave "passively" (i.e. the atmospheric circulation will be as if the injection did not occur). Sections 3.2.3-3.2.2 describe several methods by which the tracers can be made "active", providing feedback to the prognostic fields of the model in a way designed to represent causal "pathways" observed in nature.

4

3.1 Sulfate formation via "toy chemistry"

Once injected into the atmosphere, SO_2 follows an oxidation chain with an end product of sulfuric acid (H_2SO_4) that condenses with water vapor to form sulfate aerosol particles (Bekki, 1995), which has a removal timescale much longer than SO_2 of one year (Barnes & Hofmann, 1997). This aerosol is responsible for much of the heating that perturbs the Earth's energy balance and atmospheric circulation after a stratospheric volcanic eruption (McCormick et al., 1995; Robock, 2002).

In climate models with high-complexity, this process is mediated by chemistry, radiation, and moist subgrid processes. Here, we replace all of this by a direct, analytic coupling from SO_2 to sulfate, in a way inspired by the so-called "toy chemistry" of Lauritzen et al. (2015). The SO_2 sink $R(m_{SO2})$ retains the form of Eq.(2) and e-folding time k_{SO2}, but is now viewed as a reaction rate which provides a sulfate source.

The sulfate tendency mass is therefore

$$\frac{\partial m_{\text{sulf}}}{\partial t} = -k_{\text{sulf}}m_{\text{sulf}} + wk_{\text{SO2}}m_{\text{SO2}} \tag{20}$$

Or, in terms of mixing ratio discretized onto the grid:

$$\frac{\partial q_{\text{sulf},i,k}}{\partial t} = -k_{\text{sulf}}q_{\text{sulf},i,k} + wk_{\text{SO2}}q_{\text{SO2},i,k} \tag{21}$$

Here, the reaction weight w encodes the net production of sulfate per unit mass of SO_2.

In practice, w can be a tuning parameter of the model, but we can inform a first choice for it from chemistry. Since the overall effect of the oxidation sequence yields one aerosol "particle" of sulfate per molecule of SO_2 (Bekki, 1995), w will just be the ratio of the sulfate to SO_2 molar mass. It is known from observation that sulfate particles vary in their composition across latitude, altitude, and season (Yue et al., 1994), dependent on availability of water vapor, and temperature. In principle, this should complicate a realistic choice of w. We make the simplifying assumption that all sulfate particles are 75% H_2SO_4 by mass, as in Bekki (1995), and suggested by observation (Rosen, 1971; Yue et al., 1994). Defining this percentage as $f_{\text{acid}} = 0.75$, and the molar masses of H_2SO_4 and SO_2 as w_{H2SO4} and w_{SO2}, the reaction weighting is

$$w = \frac{w_{\text{H2SO4}}/f_{\text{acid}}}{w_{\text{SO2}}} \approx \frac{1/0.75 \times 98.079 \text{ g/mol}}{64.066 \text{ g/mol}} = 2.04 \tag{22}$$

In the analytic (advection-free) solution to the tracer evolution described in Section 5, this choice of w results in a peak sulfate mass of about ~28 Mt occurring ~2 months after injection. This is consistent with previous modeling efforts by e.g. Bluth et al. (1997). In that study, however, the authors note that the observed AOD anomalies post-Pinatubo lagged behind the sulfate loading, in the case that the sulfate production is modeled as a direct consequence of SO_2 depletion.

Toohey et al. (2016) (hereafter EVA v1.0) also model the $SO_2 \rightarrow$ sulfate conversion directly, but show that the sulfate mass and CCMI AOD peaks can be matched in time by tuning $k_{\text{SO2}} = 1/180$ days^{-1} . This differs markedly from the measured timescale of the post-Pinatubo SO_2 removal (Guo et al., 2004b); the claim is that this modified e-folding time is representing the *net* timescale of the entire SO_2 oxidation chain that arrives at H_2SO_4, which explains the signal lag observed in Bluth et al. (1997). Under this condition, the recovered sulfate mass peaks at ~13 Mt after 6

months. In Figure 1, we show the analytic solution to the "pulse injection" of sulfate mass from EVA v1.0, with both their choice of k_{SO2}, and ours, which shows that the difference in peak sulfate mass is explained only by this parameter choice, and not the reaction normalization.
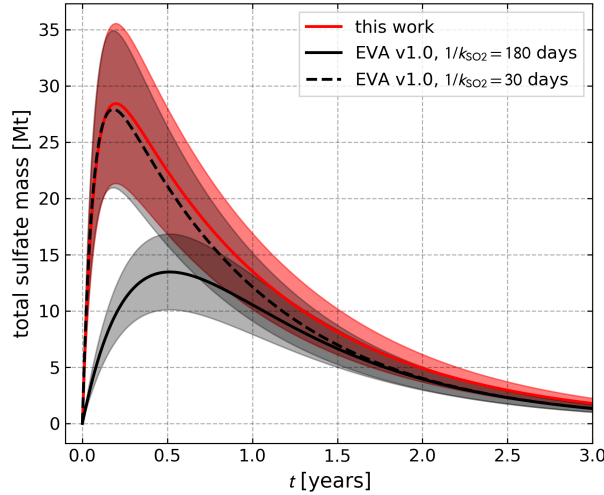
Figure 1: Total sulfate mass time series from the analytic solutions of our model (red solid line), and those from EVA v1.0 with $1/k_{SO2} = 180$ days (their default; solid black line), and an adjustment $1/k_{SO2} = 30$ days (our default; dashed black line). The adjustment of this parameter fully explains the difference in the peak mass, and all curves begin to converge after 1 year. The red curve remains largest in mass value since our e-folding timescale of sulfate (360 days) is longer than EVA v1.0 (330 days). The bands about each curve are $\pm 25\%$ of the mass value, which is the approximate uncertainty in the (Guo et al., 2004b) measurement of the initial SO_2 loading; the amplitude uncertainty in produced sulfate should be at least this much.

3.2 Diabatic forcing

3.2.1 Shortwave, longwave flux densities

In the Held-Suarez model and its variants, all radiative and convective effects are parameterized very simply via a single temperature relaxation as

$$\frac{\partial}{\partial t} = -k_t(\phi, p) \left[T - T_{\text{eq}}(\phi, p) \right] \tag{23}$$

where the "equilibrium profile" is

$$T_{\text{eq}}(\phi, p) = \max \left[200\text{K}, \left[315\text{K} - (60\text{K}) \sin^2 \phi - (10\text{K}) \log \left(\frac{p}{p_0} \right) \cos^2 \phi \right] \left(\frac{p}{p_0} \right)^\kappa \right] \tag{24}$$

At the reference pressure $p_0 = 1000$ hPa, this reduces to

$$T_{\text{eq}}(\phi, p_0) = 315\text{K} - (60\text{K}) \sin^2 \phi \tag{25}$$

We emphasize that the HS forcing set knows nothing about the radiative processes of the atmosphere other than this temperature relaxation, which is constant. That is, TOA energy balance is implied, though nothing is ever said about shortwave or longwave fluxes.

However, in computing the diabatic heating and cooling terms of the following sub-sections, it will be both convenient and natural to have average flux densities for the shortwave and longwave bands. Our strategy will be to first define a longwave flux density based on the HSW temperature equilibrium at the surface, and then deduce a shortwave component by setting the total integrated global power equal to that of the longwave component. This again implies a TOA energy balance, though this is not strictly needed, since this "radiation" will be used *only* to control the heating and cooling rates due to the injected aerosols, while the overall climate is still controlled in the standard HS way.

The longwave flux density is computed simply from the Stefan-Boltzman law, assuming the planet's surface is a graybody,

$$I_{\text{LW}} = \sigma T_{\text{surf}}^4 \tag{26}$$

where σ is the Stefan-Boltzman constant, and we assume unit emissivity. If desired, T_{surf} can be the actual surface temperature on a 2D surface mesh. However, if these datasets will ultimately be used for validation of climate attribution tools, then it may be preferable for this term to remain purely analytic. To this end, we choose to approximate the surface temperature by Eq.(25) computed at the reference pressure $p = p_0$, i.e. $T_{\text{surf}} \approx T_{\text{eq}}(\phi, p_0)$, in which case the longwave flux density is a function only of latitude:

$$I_{\text{LW}} = \sigma \left[315\text{K} - (60\text{K}) \sin^2 \phi \right]^4 \tag{27}$$

For incident shortwave radiation, we will use a simple $\cos \phi$ form:

$$I_{\text{SW}} = I_0 \cos \phi \tag{28}$$

As suggested, we will now scale I_0 by enforcing that the total globally-integrated power is in balance between I_{LW} and I_{SW} (that is, we assume that *all* longwave radiation reaches the TOA in the absence of absorption by the tracers). In what follows, r_e is the radius of the earth. The total longwave power is

$$P_{\text{LW}} = \int_0^{2\pi} \int_{-\pi/2}^{\pi/2} I_{\text{LW}} r_e^2 \cos \phi d\phi d\lambda \tag{29}$$

$$= \int_0^{2\pi} \int_{-\pi/2}^{\pi/2} \sigma \left[315\text{K} - (60\text{K}) \sin^2 \phi \right]^4 r_e^2 \cos \phi d\phi d\lambda \tag{30}$$

$$= 4\pi \sigma r_e^2 \times \left(7736342625 \, \text{K}^4 \right) \ \text{W} \tag{31}$$

$$\tag{32}$$

and the total shortwave power is

$$P_{\text{SW}} = \int_0^{2\pi} \int_{-\pi/2}^{\pi/2} I_{\text{SW}} r_e^2 \cos \phi d\phi d\lambda \tag{33}$$

$$= \int_0^{2\pi} \int_{-\pi/2}^{\pi/2} I_0 r_e^2 \cos^2 \phi d\phi d\lambda \tag{34}$$

$$= \pi^2 r_e^2 I_0 \ \text{W} \tag{35}$$

I_0 is thus

$$P_{\text{LW}} = P_{\text{SW}} \tag{36}$$

$$\implies I_0 = \frac{4\pi\sigma r_e^2 \times \left(7736342625\,\text{K}^4\right)}{\pi^2 r_e^2} = 558.54\ \frac{\text{W}}{\text{m}^2} \tag{37}$$

With this, Eqs.(27, 28) are shown in Figure 2.

This figure shows an energy deficit poleward of 55°, and a surplus equatorward, with maxima in the net flux in the midlatitudes. Having said this, we note again that this balance has been done for consistency and completeness only, and will have *no* effect on mean atmospheric temperatures. It is simply that I_{SW} will be used to scale surface cooling by the aerosol AOD, and I_{LW} will be used to scale local heating of the stratosphere. Further, we note that these fluxes are considerably higher that the annual average solar insolation of the real Earth system; this is primarily because we assume that no attenuation of the upwelling longwave radiation occurs in the HSW atmosphere. In our idealized model, including such an effect would be arbitrary and overly-complicated. Further, we will show that the heating design has sufficient freedom in the number of tunable parameters to achieve desired heating rates without being picky about the amplitudes of I_{SW} and I_{LW}.
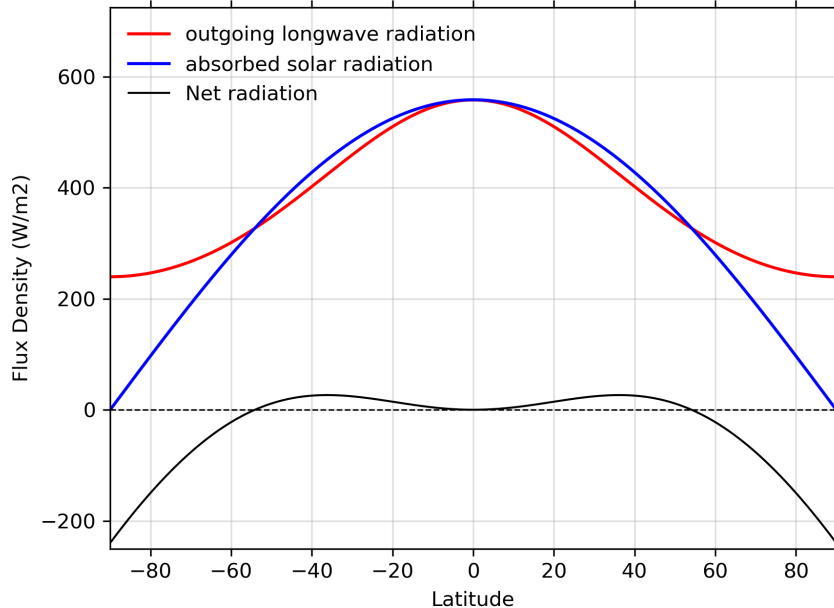
Figure 2: *Longwave and shortwave flux densities as a function of latitude. These are used to scale the aerosol heating and cooling functions; the net radiation is shown for reference only, and does not have any bearing on the atmospheric temperature, which instead has radiation parameterized solely by the Held-Suarez temperature relaxation. See text for discussion.*

3.2.2 Diabatic cooling of the surface

AOD Definition

Increased *aerosol optical depths* (AOD) decrease the flux density of shortwave solar radiation reaching the troposphere, and contributed to an observed surface cooling of ~0.5 °C during the two years following the eruption of Mt. Pinatubo (Dutton & Christy, 1992; Self et al., 1993; Fyfe et al., 2013). Here we will consider a single aerosol species, which can contribute to a reduction of transmitted radiation ("extinction") by both absorption and scattering, with magnitudes expressed via absorption and scattering coefficients β_a, β_s. The combined effect of these processes suggests the *extinction coefficient*

$$\beta_e \equiv \beta_a + \beta_s \tag{38}$$

We can express the extinction coefficient as:

$$\beta_e = b_e\rho = b_e q \rho_{atm} \tag{39}$$

where $b_e \equiv b_a + b_s$ is the *mass extinction coefficient* of the aerosol species, with dimensions of area per mass (i.e. an *extinction cross section per unit mass*), and ρ is the tracer mass density. Henceforth, we will refer to two distinct mass extinction coefficients: b_{LW} will be used for extinction of longwave radiation, which is assumed to be entirely absorption, and b_{SW} will be used for extinction of shortwave radiation, which is assumed to be entirely scattering,

$$b_{\mathrm{SW}} \equiv (b_s \text{ for the shortwave band}) \tag{40}$$

$$b_{\mathrm{LW}} \equiv (b_a \text{ for the longwave band}) \tag{41}$$

The remainder of this section will deal only in b_{SW} and b_{LW}; we do not consider any longwave involvement in the surface cooling, nor will we consider the absorption of near-IR shortwave radiation by the aerosols.

Further, within a single model column, we will make the *parallel plane approximation*, where we assume that the extinction coefficient varies only in the vertical,

$$\beta_e(x, y, z) \approx \beta_e(z). \tag{42}$$

The dimensionless *aerosol optical depth* (AOD) at a height z with model top z_{top} is then obtained by integrating the extinction:

$$\tau(z) \equiv \int_z^{z_{\mathrm{top}}} \beta_e(z')dz' \tag{43}$$

$$= \int_z^{z_{\mathrm{top}}} b_{\mathrm{SW}}\rho(z')dz' \tag{44}$$

$$= \int_z^{z_{\mathrm{top}}} b_{\mathrm{SW}}q(z')\rho_{atm}(z')dz' \tag{45}$$

When discretized onto a grid with pressure levels k and columns i with area a_i, this becomes

$$\tau_{i,k} = \sum_{k'<k} b_{\mathrm{SW}}q_{i,k'}\rho_{\mathrm{atm},i,k'}\Delta z_{i,k'} \tag{46}$$

$$= \sum_{k'<k} b_{\mathrm{SW}}\frac{q_{i,k'}\Delta p_{i,k'}}{g} \tag{47}$$

9

where the pressure weights were obtained by the hydrostatic approximation as shown in Eq.(15)-(16), and we have assumed that the index k decreases toward the model top.

Let's also define a shorthand for the cumulative AOD at the surface as $\tau_i \equiv \tau(z = 0)$. After summing over k for this case, we see that each remaining term is just the total column mass burden M_i of the aerosol, scaled by the mass extinction coefficient b_j and column area a_i,

$$\tau_i = \sum_k b_{\text{SW}} \frac{q_{i,k} \Delta p_{i,k}}{g} = \sum_k b_{\text{SW}} \frac{q_{i,k} m_{atm,i,k}}{a_i} = b_{\text{SW}} \frac{M_i}{a_i} \tag{48}$$

Likewise, Eq(47) is a "partial column burden" scaled by b_{SW}. Note that the form Eq.(48), and it's derivation, is consistent with Eq.(7.19) of Petty (2006).

We can now make a preliminary constraint of b_{SW}, such that the resulting τ_i are representative of post-Pinatubo observations. Zonal-mean AODs observed in the months and years following the Pinatubo eruption peaked near 0.2-0.5 (Toohey et al., 2016; Mills et al., 2016; Stenchikov et al., 2021; Dutton & Christy, 1992; Stenchikov et al., 1998), and passive runs of our injection protocol described in Section 2 yield maximum zonal-mean column mass burdens (as a sum of all species) which peak near 2×10^7 kg approximately 3 weeks post-injection near the equator. This suggests

$$\tau_i = 0.2 = b_{\text{SW}} \frac{M_i}{a_i} \tag{49}$$

$$\implies b_{\text{SW}} = \frac{0.2 a_i}{2 \times 10^7 \text{ kg}} \tag{50}$$

$$= 400 \ \frac{\text{m}^2}{\text{kg}} \tag{51}$$

where we took $a_i = (200 \times 200) \text{ km}^2$, consistent with a ~2 degree resolution near the equator. Before continuing, a quick sanity check of this coefficient; if the 2×10^7 of aerosol were distributed evenly over a 20 km thick section of the column (the lower to middle stratosphere), then the corresponding linear attenuation coefficient β_{SW} would be

$$\beta_{\text{SW}} = b_{\text{SW}} \rho_i = \frac{\left(400 \text{ m}^2/\text{kg}\right) \left(2 \times 10^7 \text{ kg}\right)}{a_i \left(20 \text{ km}\right)} = 1 \times 10^{-5} \ \frac{1}{\text{m}} \tag{52}$$

Surface Cooling

We model the surface cooling as an AOD attenuation of an incident radiation with flux density I_{SW}, as defined in Eq.(28). If this radiation propagates toward the surface along a path s, then by the *Beer-Lambert law*, the attenuated flux is

$$I = I_{\text{SW}} \exp \left(- \int_{s_1}^{s_2} \beta_e(s) ds \right) \ \frac{\text{W}}{\text{m}^2} \tag{53}$$

Again taking the parallel plane approximation, and assuming that radiation from the sun is always directly overhead, the path of propagation becomes $s \to z$, and thus $\beta_e(s) \to \beta_e(z)$. The integral
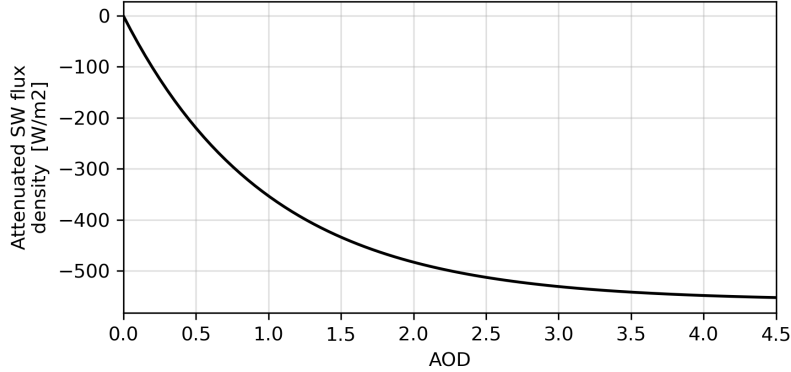
Figure 3: *Shortwave attenuation ΔI_i of Eq.(56) with respect to aerosol optical depth τ. The attenuation, and thus the associated surface cooling, saturates (scatters all available incident radiation) by $\tau \approx 4$*

term in brackets is then exactly the AOD as derived in the previous section. This gives the attenuation for a horizontally-uniform column as

$$I(z) = I_{\mathrm{SW}}\exp\left(-\int_z^{z_{\mathrm{top}}} \beta_e(z')dz'\right) = I_{\mathrm{SW}}e^{-\tau(z)} \ \frac{\mathrm{W}}{\mathrm{m}^2} \tag{54}$$

The deficit intensity after attenuation by the aerosol over the full height of the atmosphere is then

$$\Delta I \equiv I(z=0) - I_{\mathrm{SW}} = I_{\mathrm{SW}}\left(e^{-\tau(z=0)} - 1\right) \ \frac{\mathrm{W}}{\mathrm{m}^2} \tag{55}$$

With the notation used in Eq.(48), discretized onto a single grid column i, this is

$$\Delta I_i = I_{\mathrm{SW}}\left(e^{-\tau_i} - 1\right) \ \frac{\mathrm{W}}{\mathrm{m}^2} \tag{56}$$

That is, extinction by the aerosol population in this column imposes a deficit of ΔI_i watts per each square meter of the column in the horizontal. By taking I_{SW} at $\phi = 0$, according to Eq.(28), and $\tau = 0.2$, this form gives $\Delta I \approx -100 \ \mathrm{W/m^2}$, which is roughly consistent with the observed broadband solar transmission deficits of ~20% in the months following Pinatubo (Self et al., 1993). Also note that since ΔI_i is exponential, the shortwave attenuation will saturate by AODs of $\tau \approx 4$, as shown in Figure 3 Since τ scales linearly with the column mass M_i, we can expect the cooling effect to saturate as well for column masses of $4/0.2 = 20$ times the initial injection of the tuning run (recall, a maximum column burden of 2×10^7 with $\tau = 0.2$). With the rapid dilution of the tracer densities by advection, it is difficult to say if this means that the cooling effect will also saturate if the initial SO_2 mass loading is increased by a factor of 20. Double checking that the surface cooling rate is as expected is advised when running with injection masses of this magnitude.

We now need to translate this to a cooling rate per unit mass s^{surf}, and associated daily temperature tendency ΔT. Let us assume that *all* of the energy lost over the column *would have* heated the planetary surface, which in turn would have transferred heat to the atmosphere by a function F with some efficiency ζ:

$$s_{i,k}^{\mathrm{surf}} = \zeta F(\Delta I_i) \tag{57}$$

11

The "efficiency" ζ can be interpreted as an actual heat transfer efficiency, or difference in the heat transfer rates between radiation, the surface, and the atmosphere, an expression of the difference of specific heat capacities of the surface and atmosphere, etc... We consider it a catch-all for any of these effects which we do not model, and will treat it as a tuning parameter for the magnitude of atmospheric surface cooling.

The function F can be obtained by dimensional analysis:

$$s_{i,k}^{\text{surf}} = \zeta \frac{a_i \Delta I_i}{m_i^{\text{cool}}} \frac{\text{J}}{\text{kg s}} \tag{58}$$

$$\implies \Delta T_{i,k} = \zeta \frac{1}{c_p} \frac{a_i \Delta I_i}{m_i^{\text{cool}}} \frac{(1 \text{ day})}{(86400 \text{ s})} \frac{\text{K}}{\text{day}} \tag{59}$$

where m_i^{cool} is the mass of air in the lowest n model levels over which the cooling is desired to be applied. If we apply the cooling only to the lowest model level, i.e. $n = 1$, then

$$m_i^{\text{cool}} = m_{i,k=n_{\text{lev}}} \tag{60}$$

and otherwise

$$m_i^{\text{cool}} = \sum_{k=n_{\text{lev}}}^{n_{\text{lev}}-(n-1)} m_{i,k} \tag{61}$$

In this way, the net cooling (total energy loss in J over unit time) is conserved as n increases, and the cooling per unit mass is "diluted". The choice of n will effectively encode whatever missing physical mechanisms should communicate the cooling higher in the vertical column; choosing $n = 1$ supposes that heat exchange from the surface and atmosphere is primarily by conduction, or rapidly attenuating radiative transfer. In principle, convection should distribute this heating in the vertical; we could attempt to account for this by setting $n > 1$, or instead leave the treatment of convection to the model configuration. For $n > 1$, $\Delta T_{i,k}$ and $s_{i,k}^{\text{surf}}$ are 3D quantities, while ΔI_i and τ_i are always 2D quantities. In Table 1, rather than setting n directly we set δz_{cool}, or the height above the surface in meters where the cooling should be applied, which contains n model levels, depending on the vertical discretizaiton.

Now, we can use Eq.(56) to make a preliminary tuning of ζ. Stenchikov et al. (2021) informs us that peak spatial-mean values of the surface cooling in the equatorial belt from 0°-15°N post-injection are around -0.02 K/day. In this region, we have already roughly constrained τ to be near 0.2 in Eq.(51). Making use of Eq.(59):

$$\left(-0.02 \ \frac{\text{K}}{\text{day}}\right) = \zeta \frac{1}{c_p} \frac{a_i}{m_{i,\text{surf}}} \frac{(1 \text{ day})}{(86400 \text{ s})} I_{\text{SW}} \left(\exp(-0.2) - 1\right) \tag{62}$$

$$\implies \zeta^{-1} = \frac{1}{c_p} \frac{a_i}{m_{i,\text{surf}}} \frac{(1 \text{ day})}{(86400 \text{ s})} \frac{1}{\left(-0.02 \ \frac{\text{K}}{\text{day}}\right)} I_{\text{SW}} \left(\exp(-0.2) - 1\right) \tag{63}$$

Using I_{SW} from Eq.(28) at latitude $\phi = 0$, and $m_{i,\text{surf}}$ from Eq.16 with $\Delta p_{i,k} = 20$ hPa (corresponding to ~200 meters or $n = 3$ for Eq.(61) in E3SM), this gives

$$\zeta \approx 4.7 \times 10^{-4} \tag{64}$$

which is independent of horizontal resolution, since a_i cancels in Eq.(63) (though it is dependent on vertical resolution).

3.2.3 Diabatic heating of the stratosphere

In addition to cooling the surface remotely via scattering of solar radiation, the presence of SO_2 and sulfate in the stratosphere also induces a local diabatic heating to the temperature field by absorption of upward-propagating longwave radiation [citations needed]. After the Mt. Pinatubo eruption, this process resulted in a temperature anomaly of up to ~3-4 K peaking near 50-30 hPa [citations needed], driven by a maximum net temperature change at a rate of ~1 K/month during the initial period following the injection, and subsequent plateau for nearly a year (see Mills et al. (2016), Figure 2).

We model this local warming effect similarly to the cooling of Section 3.2.2, as an attenuation of upwelling longwave radiation with flux density I_{LW} defined in Eq.(27). This time, we will write the plane-parallel Beer-Lambert law (for a single uniform column) as an integral of the extinction β_e over the vertical bounds of a particular slab, $[z_0, z_1]$,

$$I(z_0, z_1) = I_{LW} \exp\left(-\int_{z_0}^{z_1} \beta_e(z')dz'\right) \tag{65}$$

Here we assume that z_0 is the lowest extent of the aerosol plume, and there has been no attenuation between $z = 0$ and $z = z_0$. In this case, the power per unit area absorbed by this slab is

$$\Delta I = I_{LW} - I(z_0, z_1) \tag{66}$$

$$= I_{LW}\left[1 - \exp\left(-\int_{z_0}^{z_1} \beta_e(z')dz'\right)\right] \tag{67}$$

$$\tag{68}$$

If we consider another slab located immediately above z_1, on $[z_1, z_2]$, then the incident flux is no longer I_{LW}, but rather $I(z_0, z_1)$:

$$I(z_1, z_2) = I(z_0, z_1) \exp\left(-\int_{z_1}^{z_2} \beta_e(z')dz'\right) \tag{69}$$

$$= I_{LW} \exp\left(-\int_{z_0}^{z_2} \beta_e(z')dz'\right) \tag{70}$$

and the power per unit area absorbed is

$$\Delta I = I(z_0, z_1) - I(z_1, z_2) \tag{71}$$

$$= I_{LW} \exp\left(-\int_{z_0}^{z_1} \beta_e(z')dz'\right)\left[1 - \exp\left(-\int_{z_1}^{z_2} \beta_e(z')dz'\right)\right] \tag{72}$$

$$\tag{73}$$

This is easy to generalize to an arbitrary slab on $[z_n, z_{n+1}]$ as

$$\Delta I = I(z_{n-1}, z_n) - I(z_n, z_{n+1}) \tag{74}$$

$$= I_{LW} \exp\left(-\int_{z_0}^{z_n} \beta_e(z')dz'\right)\left[1 - \exp\left(-\int_{z_n}^{z_{(n+1)}} \beta_e(z')dz'\right)\right] \tag{75}$$

$$\tag{76}$$

Discretizing this onto the vertical grid with levels k in column i in the manner of Eqs.(43-47) (being sure to use b_{LW} rather than b_{SW}) yields

$$\Delta I_{i,k} = I_{\text{LW}} \exp\left(-\sum_{k'>k} b_{\text{LW}} \frac{q_{i,k'}\Delta p_{i,k'}}{g}\right) \left[1 - \exp\left(-b_{\text{LW}}\frac{q_{i,k}\Delta p_{i,k}}{g}\right)\right] \tag{77}$$

where the leftmost exponent sums over all levels k' which are below level k. The effect here is that aerosols lower in the vertical column "shadow" those above, decreasing the power of incident radiation available for absorption; in this way, the peak of the local aerosol heating may lie below the actual density peak of the plume.

If a simpler implementation is desired, one that does not have this additional dependency on q at other vertical levels, we could instead just assume that I_{LW} is incident upon *all* levels, in which case Eq.(77) reduces to

$$\Delta I_{i,k} = I_{\text{LW}} \left[1 - \exp\left(-b_{\text{LW}}\frac{q_{i,k}\Delta p_{i,k}}{g}\right)\right] \tag{78}$$

In either case, this absorbed power (per unit area) must again be translated to a heating rate per unit mass s_{strat} in J/(kg s) and associated temperature tendency ΔT in K/day. If all of the absorbed radiation is converted to heat, then

$$s_{i,k}^{\text{strat}} = \frac{a_i \Delta I_{i,k}}{m_{i,k}} \quad \frac{\text{J}}{\text{kg s}} \tag{79}$$

$$\implies \Delta T_{i,k} = \frac{1}{c_p} \frac{a_i \Delta I_{i,k}}{m_{i,k}} \frac{(86400 \text{ s})}{(1 \text{ day})} \quad \frac{\text{K}}{\text{day}} \tag{80}$$

Further, it turns out that the exponentials in Eqs.(77) and (78) can be well approximated by linear functions:

$$\text{Eq.(77)} \rightarrow \Delta I_{i,k} = I_{\text{LW}} \left[1 - \sum_{k'>k} b_{\text{LW}}\frac{q_{i,k'}\Delta p_{i,k'}}{g}\right] \left(b_{\text{LW}}\frac{q_{i,k}\Delta p_{i,k}}{g}\right) \tag{81}$$

$$\text{Eq.(78)} \rightarrow \Delta I_{i,k} = I_{\text{LW}} \left(b_{\text{LW}}\frac{q_{i,k}\Delta p_{i,k}}{g}\right) \tag{82}$$

In general, the un-approximated functions have sigmoid-like forms, which experiences an exponential increase in $\log(q)$, before eventually saturating at very high mixing ratios when I_{LW} has been completely absorbed. In practice, we will only ever encounter mixing ratios which are well within the exponential regime (linear in q), which holds to better than 1% until at least $\log(q) = -2$ for any $\Delta p \in [0\,\text{hPa}, 40\,\text{hPa}]$ (the range spanned by E3SM). For an injection of 17 Tg SO_2, we observe maximum mixing-ratios at the girdpoint level on the order of 10^{-4}; even increasing the initial mass injection by a factor of 100 would not compromise the approximated form, so we choose to implement it. In other words, within reasonable eruption parameter choices, it is much less likely that we achieve a longwave attenuation saturation effect that we saw in the shortwave implementation, as described for the AOD in Section 3.2.2. The relative approximation error is shown as a function of q in Figure 4 for Eq.(82). ***Edit:*** I've done some more tests on the accuracy of this approximation in the single-column model described in Section 5; while Eq.(81) is the more accurate approximation,

there is actually *more* disagreement between Eqs.(77) and (81) than there is between Eqs.(78) and (82), the latter of which is (misleadingly) shown in Figure 4. I suspect this is due to the error compounding in the vertical when encountering the sum over k in Eq.(81). I still see errors on the order of ~1%, but without truly understanding the behavior of the form under more realistic conditions, I'll decide to just implement the unapproximated exponential form Eq.(77).
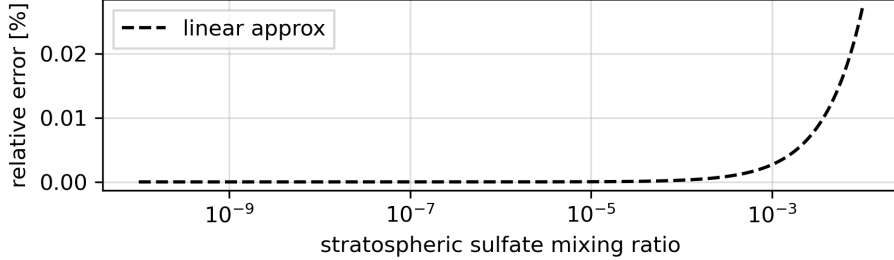
Figure 4: *The relative error of the linear approximation Eq.(82) as a function of mixing ratio, using the parameter values given in the derivation of Eq.(85).*

Finally, we can use Eq.(82) to make a preliminary tuning of b_{LW}. Stenchikov et al. (1998) informs us that peak monthly-mean zonal-mean values for the stratospheric heating rate 3-6 months post-injection are around 0.3 K/day near the equator, and passive runs of our injection protocol described in Section 2 yield monthly-mean zonal-mean mixing ratios at this time and location of about 10^{-4}. Making use of Eq.(80):

$$\left(0.3 \ \frac{\mathrm{K}}{\mathrm{day}}\right) = \frac{1}{c_p} \frac{a_i}{m_{i,k}} I_{\mathrm{LW}} \left(b_{\mathrm{LW}} \frac{q_{i,k} \Delta p_{i,k}}{g}\right) \frac{(86400 \ \mathrm{s})}{(1 \ \mathrm{day})} \tag{83}$$

$$\implies b_{\mathrm{LW}} = \frac{\left(0.3 \frac{\mathrm{K}}{\mathrm{day}}\right)}{\left(10^{-4} \ \frac{\mathrm{kg}}{\mathrm{kg}}\right)} \frac{g c_p m_{i,k}}{a_i I_{\mathrm{LW}} \Delta p_{i,k}} \frac{(1 \ \mathrm{day})}{(86400 \ \mathrm{s})} \ \frac{\mathrm{m}^2}{\mathrm{kg}} \tag{84}$$

Using $a_i = (200 \times 200 \ \mathrm{km})$, $\Delta p_{i,k} = 8 \ \mathrm{hPa}$, I_{LW} from Eq.(27) at latitude $\phi = 0$, and $m_{i,k}$ from Eq.16, this gives

$$b_{\mathrm{LW}} \approx 0.062 \ \frac{\mathrm{m}^2}{\mathrm{kg}} \tag{85}$$

Comparing this with Eq.(51), our formulation implies that the aerosols are much more efficient at attenuating shortwave radiation (by scattering) than longwave radiation (by absorption). This is consistent with earlier statements that the longwave attenuation is safe to linearly approximate, while the shortwave attenuation is not.

As a preliminary guess, all tracer species will adopt the same b_{LW}, though we identify $b_{\mathrm{LW,ash}}$ in particular as a tuning parameter of the model. This is because the lofting magnitude of the plume will be controlled by the aggressive early heating of ash in the fresh plume, since the initial ash mass loading is decisively dominant over SO_2 (see Table 1). This suggests that either the total ash burden M_{ash}, or b_{LW} for ash can serve as a the tuning parameter which will control the settling height of the aged aerosols.

15

3.2.4 Generalization to mixtures of tracer species

With multiple tracer species j introduced, the total radiative heating is not derived from a simple sum of the ΔT solutions found over the proceeding sections. Rather, it is the total extinction which is determined by additive extinction coefficients,

$$\beta_e = \sum_j \beta_{e,j} = \sum_j b_{e,j} m_j \tag{86}$$

In this case, the total AOD of Eq.(48) simply becomes

$$\tau_i = \sum_k \sum_j b_{\mathrm{SW},j} \frac{q_{j,i,k}\Delta p_{i,k}}{g} = \sum_j b_{\mathrm{SW},j} \frac{M_i}{a_i} = \sum_j \tau_{j,i} \tag{87}$$

Since the implementation of surface cooling due to shortwave extinction depends only on the total τ_i, nothing further needs to be done.

For the longwave heating, the expression is a bit more complicated; Eq.(77) becomes

$$\Delta I_{i,k} = I_{\mathrm{LW}}\exp\left(-\sum_j \sum_{k'>k} b_{\mathrm{LW},j}\frac{q_{j,i,k'}\Delta p_{i,k'}}{g}\right)\left[1-\exp\left(-\sum_j b_{\mathrm{LW},j}\frac{q_{j,i,k}\Delta p_{i,k}}{g}\right)\right] \tag{88}$$

Here, each grid cell has incident upon it radiation of a power density that has already been attenuated by *all* species j underneath it, and so this does not work out to a sum of j separate evaluations of ΔI; in this case, it is probably simplest to compute these exponents in advance.

4 Model summary

<div style="border:1px solid">

Tracer tendencies

$$\frac{\partial q_{j,i,k}}{\partial t} = \frac{g}{\Delta p_{i,k}a_i}\left[-k_j m_j + \frac{M_j}{\delta t \sum_k V_k}V_k\delta_{ii'}\right] \tag{18}$$

$$\frac{\partial q_{\mathrm{sulf},i,k}}{\partial t} = -k_{\mathrm{sulf}}q_{\mathrm{sulf},i,k} + w k_{\mathrm{SO2}}q_{\mathrm{SO2},i,k} \tag{21}$$

SW radiative and optical properties

$$I_{\mathrm{SW}} = I_0 \cos\phi \tag{28}$$

$$\tau_i = \sum_j b_{\mathrm{SW},j}\frac{M_i}{a_i} \tag{48}$$

$$\Delta I_i = I_{\mathrm{SW}}\left(e^{-\tau_i}-1\right)\ \frac{\mathrm{W}}{\mathrm{m}^2} \tag{56}$$

$$s_{i,k}^{\mathrm{surf}} = \zeta\frac{a_i\Delta I_i}{m_i^{\mathrm{cool}}}\ \frac{\mathrm{J}}{\mathrm{kg\ s}} \tag{58}$$

LW radiative and optical properties

$$I_{\mathrm{LW}} = \sigma\left[315\mathrm{K} - (60\mathrm{K})\sin^2\phi\right]^4 \tag{27}$$

$$\Delta I_{i,k} = I_{\mathrm{LW}}\exp\left(-\sum_j\sum_{k'>k}b_{\mathrm{LW},j}\frac{q_{j,i,k'}\Delta p_{i,k'}}{g}\right)$$
$$\times\left[1-\exp\left(-\sum_j b_{\mathrm{LW},j}\frac{q_{j,i,k}\Delta p_{i,k}}{g}\right)\right] \tag{77}$$

$$s_{i,k}^{\mathrm{strat}} = \frac{a_i\Delta I_{i,k}}{m_{i,k}}\ \frac{\mathrm{J}}{\mathrm{kg\ s}} \tag{79}$$

Box 1: *Summary of the important model equations controlling the tracer injection and removal, and radiative and optical properties for the tracers in shortwave and longwave broadbands. See equation numbers and text for explanations.*

</div>

Table 1: *Model parameters. Parameters with a superscript † are tuned parameters. Parameters with a superscript ‡ are constrained by a data-driven calculation, though not necessarily free for tuning. Parameters without a superscript are observations and/or estimates directly from the literature.*

Parameter	Value	Units	Description	Reference
injection parameters				
ϕ_0	15.15	deg	meridional plume center	
λ_0	120.35	deg	zonal plume center	
δt	24	hr	injection duration	
μ	14	km	peak injection altitude	Stenchikov et al. (2021)
tracer parameters				
k_{SO2}	1/25	1/day	SO_2 decay rate	Guo et al. (2004b)
$k_{sulfate}$	1/360	1/day	sulfate decay rate	Barnes and Hofmann (1997)
k_{ash}	1	1/day	ash decay rate	Guo et al. (2004a)
M_{SO2}	17	Tg	injected mass of SO2	Guo et al. (2004b)
M_{ash}	50	Tg	injected mass of ash	Guo et al. (2004a)
$w^{\ddagger}$	2.04	-	$SO_2 \rightarrow$ sulfate weighting	See Section 3.1
heating parameters				
$\zeta^{\dagger}$	4.0×10^{-3}	-	surface heating efficiency	See Section 3.2.2
$\delta z_{cool}^{\dagger}$	100	m	max height of surf. cooling	See Section 3.2.2
b_{SW}, ash, $SO_2^{\ddagger}$	400	m²/kg	SW mass extinction coeff.	See Section 3.2.2
b_{SW}, sulfate‡	1900	m²/kg	SW mass extinction coeff.	See Section 3.2.2
b_{LW}, $SO_2^{\dagger}$	0.01	m²/kg	LW mass extinction coeff.	See Section 3.2.3
b_{LW}, sulfate†	29	m²/kg	LW mass extinction coeff.	See Section 3.2.3
b_{LW}, ash†	1×10^{-5}	m²/kg	LW mass extinction coeff.	See Section 3.2.3

5 Single-column analytic solution

In the absence of advection, the evolution of the tracer mass $m_j(t)$ in column i is solvable analytically, and the partial derivatives $\partial/\partial t$ used in the previous sections become material derivatives d/dt. Recall from Section 2 that for the fixed vertical position z', we have

$$\frac{dm_j}{dt} = -k_j m_j(t) + f(t), \tag{89}$$

Obtaining $m_j(t)$ is an initial-value problem of this first-order linear ODE for $m_j(t)$ with $m_j(t_0) = 0$ (recall that t_0 is the initial injection time). In the likely event that we do not remember ODE solution methods from our time as an undergraduate, we can recruit Mathematica, which gives

$$m_j(t) = \frac{A_j V(z')}{k_j} e^{-k_j t'} \left(e^{k_j t_{\min}} - 1 \right) \tag{90}$$

where we have defined

$$t' = t - t_0, \tag{91}$$

$$t_{\min} = \min[t', \delta t] \tag{92}$$

Of course, any evaluation of these solutions will require a choice of vertical discretization to compute the normalization A, or in the continuum, we can replace the pmf $\sum_k V_k \mathrm{km}^{-1}$ with the integrated pdf $\int_0^\infty V(z) dz$.

We can now use this solution to verify the "toy chemistry" sulfate formation implementation. In the absence of advection, and with the choices $k_{\mathrm{sulf}} = 0$ and $w = 1$, Eq.(20) should give rise to a sulfate mass which reaches an enduring steady state equaling the total input SO_2 mass; let us call this quantity $\overline{m}_{\mathrm{sulf}}$. With these constraints, the total sulfur-species mass $m_{\mathrm{SO2}}(t) + \overline{m}_{\mathrm{sulf}}(t)$ should be conserved once the injection is complete ($t' > \delta t$). The mass m_{SO2} is given by Eq.(90), which means

$$\frac{d}{dt}\overline{m}_{\mathrm{sulf}}(z, t) = k_{\mathrm{SO2}} m_{\mathrm{SO2}}$$
$$= A_{\mathrm{SO2}} V(z) e^{-k_{\mathrm{SO2}} t'} \left(e^{k_{\mathrm{SO2}} t_{\min}} - 1 \right) \tag{93}$$

Integrating this (while keeping in mind to handle the piecewise inheritance from $t_{\min}$) gives the sulfate mass as

$$\overline{m}_{\mathrm{sulf}} = \frac{A_{\mathrm{SO2}} V(k)}{k_{\mathrm{SO2}}} e^{-k_{\mathrm{SO2}} t'} \left(1 - e^{k\mathrm{SO2} t_{\min}} + e^{k_{\mathrm{SO2}} t'} k_{\mathrm{SO2}} t_{\min} \right) \tag{94}$$

Taking $t_{\min} \to t_f$ allows us to verify the post-injection mass conservation:

$$m_{\mathrm{SO2}}(t) + \overline{m}_{\mathrm{sulf}}(t) = \frac{A_{\mathrm{SO2}} V(z)}{k_{\mathrm{SO2}}} e^{-k_{\mathrm{SO2}} t'} \left(e^{k_{\mathrm{SO2}} \delta t} - 1 \right) +$$
$$\frac{A_{\mathrm{SO2}} V(k)}{k_{\mathrm{SO2}}} e^{-k_{\mathrm{SO2}} t'} \left(1 - e^{k\mathrm{SO2} \delta t} + e^{k_{\mathrm{SO2}} t'} k_{\mathrm{SO2}} \delta t \right)$$
$$= \frac{A_{\mathrm{SO2}} V(k)}{k_{\mathrm{SO2}}} e^{-k_{\mathrm{SO2}} t'} \left[\left(1 - e^{k\mathrm{SO2} \delta t} + e^{k_{\mathrm{SO2}} t'} k_{\mathrm{SO2}} \delta t \right) + \left(e^{k_{\mathrm{SO2}} \delta t} - 1 \right) \right]$$
$$= \frac{A_{\mathrm{SO2}} V(k)}{k_{\mathrm{SO2}}} e^{-k_{\mathrm{SO2}} t} e^{k_{\mathrm{SO2}} t} k_{\mathrm{SO2}} \delta t$$
$$= A_{\mathrm{SO2}} V(k) \delta t = \mathrm{const.} \tag{95}$$

For completeness, the advection-free solution $m_{\mathrm{sulf}}(t)$ for arbitrary w and k_{sulf} is

$$m_{\mathrm{sulf}}(t) = \frac{w A_{\mathrm{SO2}} V(k)}{(k_{\mathrm{sulf}} - k_{\mathrm{SO2}}) k_{\mathrm{sulf}}} e^{-k_{\mathrm{sulf}} t'} \times$$
$$\left[k_{\mathrm{SO2}} \left(1 - e^{k_{\mathrm{sulf}} t_{\min}} \right) - k_{\mathrm{sulf}} e^{(k_{\mathrm{sulf}} - k_{\mathrm{SO2}}) t'} \left(1 - e^{k_{\mathrm{SO2}} t_{\min}} \right) \right] \tag{96}$$

In Figure 5, the mass evolution of each tracer across time is shown in the injection column, given by Eq.(90) and Eq.(96), assuming the parameter choices of Table 1 and a grid cell area of $(140 \times 140$ m$^2)$. The non-decaying sulfate solution Eq.(94) is also shown, providing a visual confirmation that

18
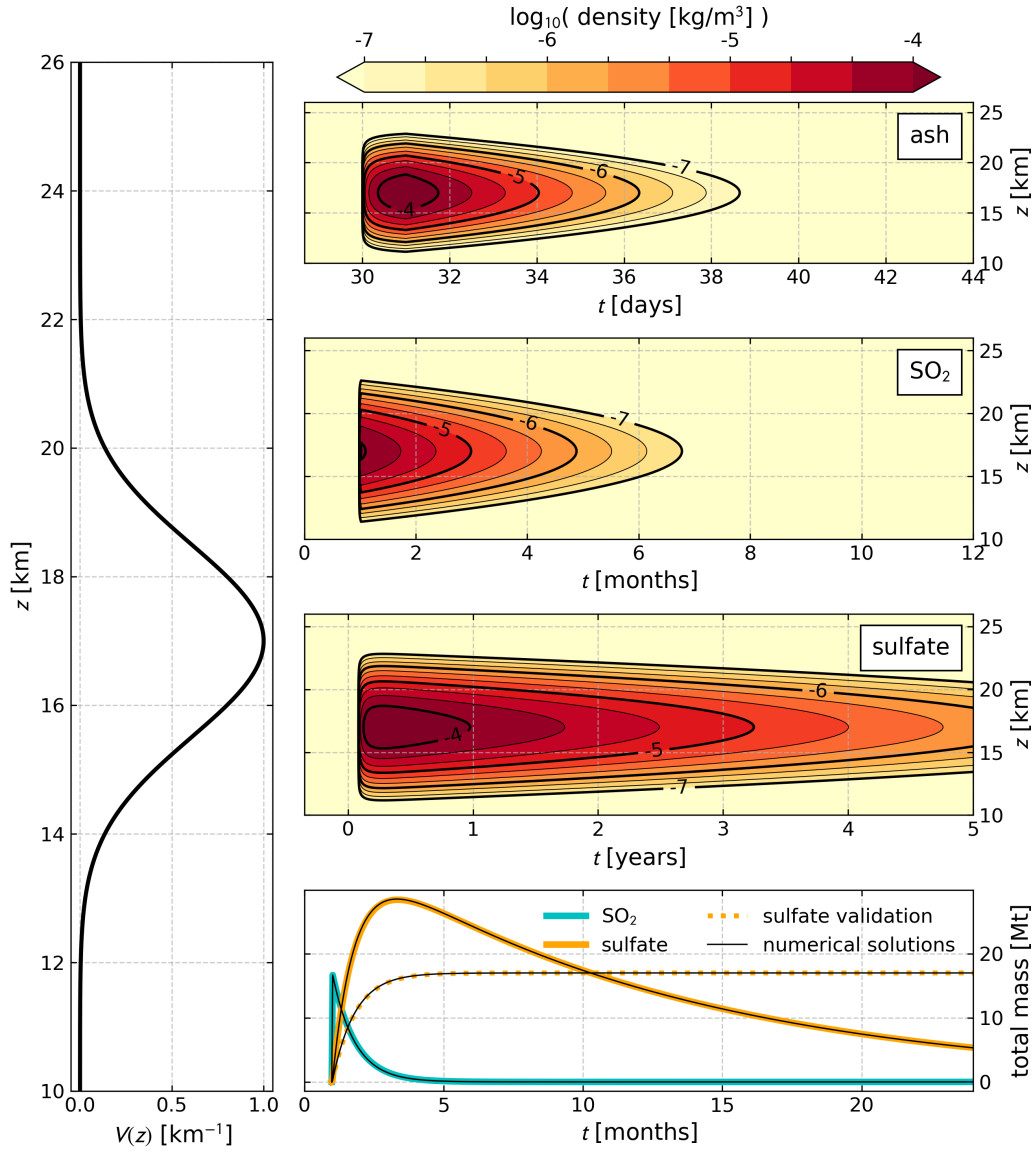
Figure 5: *The analytic (single-column, advection-free) solution to the parameterized injection and $SO_2 \rightarrow$ sulfate reaction given the parameter choices presented in Table 1. The time of injection is $t = 30$ days. (left) the vertical profile Eq.(19) described in Section 2. (right) contour plots show the ash, SO_2, and sulfate densities according to Eqs.(90, 96), assuming a column area of $a_i = 200^2$ km^2. Differing grid cell areas (resolution) will change the tracer densities in the column, but not the total tracer mass. (bottom right) total SO_2 and sulfate masses according to Eq.(90) and Eq.(96). Also shown is a "sulfate validation" curve, which solves Eq.(94), and conserves the total injected SO_2 mass (see text). Thin black lines give numerical (explicit first-order) solutions to the SO_2 and sulfate tendencies, verifying the analytic solutions.*

19
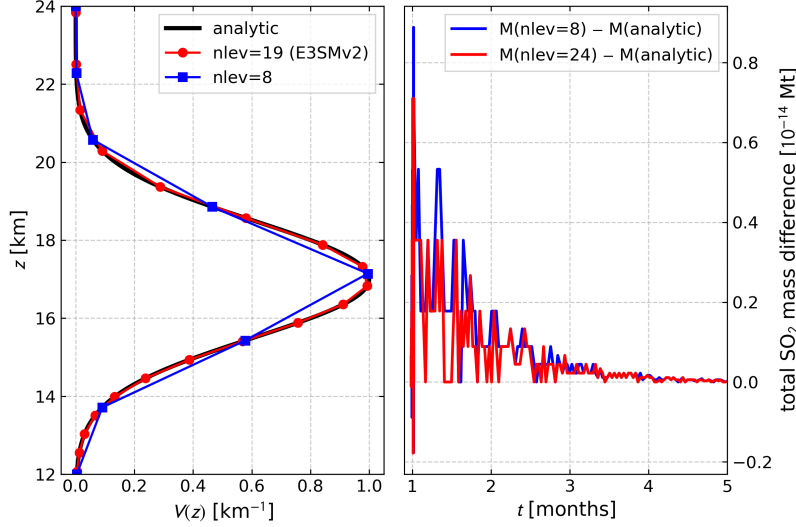
Figure 6: *Verification of the discretized form for the normalization constant A_{SO2} as defined in Eq.(12). Two vertical discretizations are shown with nlev levels distributed from 12 km to 24 km. The nlev= 19 curve gives the positions of the E3SMv2 levels in this region, where the z is the geopotential height above the surface as output from the model in the HSW configuration. (left) the sampling of the profile $V(z)$ (right) difference of the total SO2 mass across time between the nlev=8, 19 profiles, and the analytic reference, computed via Eq.(90). The differences are on the order of machine precision.*
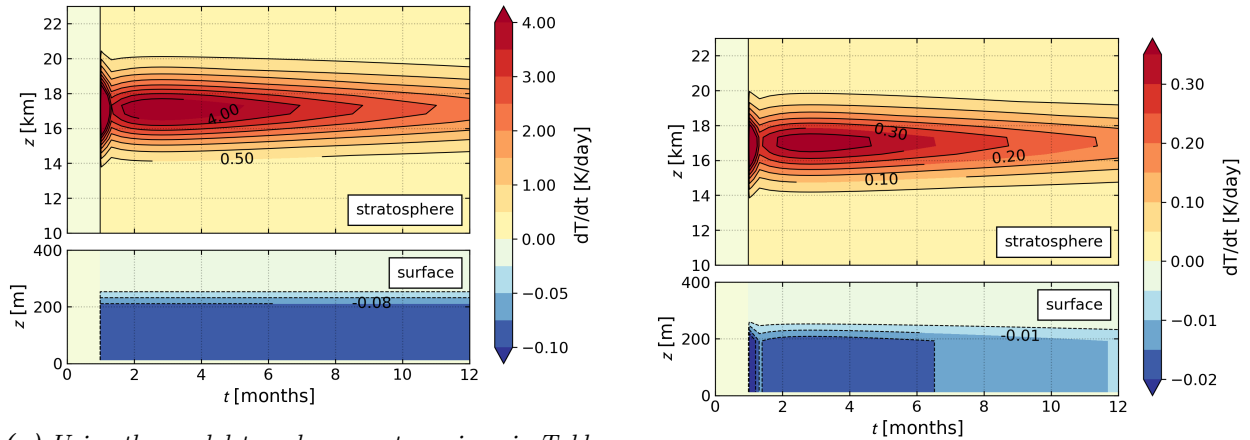
(a) *Using the model-tuned parameters given in Table 1. Heating rates are an order of magnitude higher than intended, and the surface cooling has saturated due to high AOD values. See text for discussion.*

(b) *Re-tuning the SW and LW mass extinction coefficients to mimic the heating rates of observations in the single-column. See text for discussion.*

Figure 7: *The temperature tendencies due to radiative heating, Eqs.(59, 80), for the advection-free single-column injection model. Calculations were done assuming $\phi = 15°$, and a grid cell area of (200×200) km^2. The surface cooling is applied to all levels below 200 m, which for E3SM is the three lowest model levels. Air masses were estimated using the US Standard Atmosphere (U.S. Standard Atmosphere, 1976, 1976).*

the function balances the SO_2 removal. Overplotted are numerical solutions (explicit first-order) of the mass tendency ODE, which verify the analytic solutions. Figure 6 shows the same total SO_2 and sulfate mass evolution as in Figure 5, with three differing vertical discretizations. This verifies that the normalization is insensitive to this choice, as discussed in Section 2.

Finally, Figure 7a shows the combined stratospheric heating (Section 3.2.3) and surface cooling (Section 3.2.2) of the column across a year of time. In this case, the parameters followed the defaults of Table 1, which were tuned to qualitatively match the heating rates of Stenchikov et al. (1998) (see their Plate 5), featuring maximum temperature rates of change as ~0.3 K/day in the stratosphere, and ~-0.01 K/day at the surface for several months following the injection.

Because parameter tuning was done with respect to the real model, where mixing ratios are drastically lowered in the injection column by horizontal transport, the heating rates for the single-column test shown in Figure 7a are substantially higher than this (both the heating and cooling magnitude by nearly ten fold), which is expected– as mentioned in Section 3.2.2, when embedded in the GCM, the maximum column burden of all species is near 2×10^7 kg, while the single-column model sees burdens in excess of 3×10^{10} kg for the same initial SO_2 injection. Notice also that shortwave radiation experiences the attenuation saturation discussed in Section 3.2.2, since the peak AOD with this very high column mass is $\gg 4$, which results in a constant surface cooling for the entire time domain shown. If we re-tune b_{SW} (in the manner of Eqs.(51)) against the peak mass seen for the single column, then the surface cooling avoids saturation, and diminishes along with the stratospheric heating. This effect is shown in Figure 7b; here both the SW and LW mass extinction coefficients have been re-tuned to yield heating rates that mimic the observational targets. This single-column model is, if nothing else, a nice environment for testing how sensitive the heating forms are to changes in the relevant parameters.

Finally, we note that the single column model of course does not experience the self-lofting by radiative heating of ash, and so eternally remains at the peak injection altitude, while in the full model, the plume will quickly become buoyant and rise, also acting to decrease local mixing ratios.

References

Barnes, John E. and David J. Hofmann (1997). "Lidar measurements of stratospheric aerosol over Mauna Loa Observatory". In: *Geophysical Research Letters* 24.15, pp. 1923–1926. DOI: 10.1029/97GL01943.

Bekki, S. (1995). "Oxidation of volcanic SO2: A sink for stratospheric OH and H2O". In: *Geophysical Research Letters* 22.8, pp. 913–916. DOI: 10.1029/95GL00534.

Bekki, S. and J. A. Pyle (1994). "A two-dimensional modeling study of the volcanic eruption of Mount Pinatubo". In: *Journal of Geophysical Research: Atmospheres* 99 (D9), pp. 18861–18869. DOI: 10.1029/94JD00667.

Bluth, Gregg J. S. et al. (Nov. 1997). "Stratospheric Loading of Sulfur from Explosive Volcanic Eruptions". In: *The Journal of Geology* 105.6, pp. 671–684. DOI: 10.1086/515972.

Dutton, Ellsworth G. and John R. Christy (1992). "Solar radiative forcing at selected locations and evidence for global lower tropospheric cooling following the eruptions of El Chichón and Pinatubo". In: *Geophysical Research Letters* 19.23, pp. 2313–2316. DOI: 10.1029/92GL02495.

Fisher, Bradford L. et al. (Sept. 25, 2019). "A new discrete wavelength backscattered ultraviolet algorithm for consistent volcanic SO2 retrievals from multiple satellite missions". In: *Atmospheric Measurement Techniques* 12.9, pp. 5137–5153. DOI: 10.5194/amt-12-5137-2019.

Fyfe, J. C. et al. (2013). "Surface response to stratospheric aerosol changes in a coupled atmosphere–ocean model". In: *Geophysical Research Letters* 40.3, pp. 584–588. DOI: 10.1002/grl.50156.

Guo, Song et al. (2004a). "Particles in the great Pinatubo volcanic cloud of June 1991: The role of ice". In: *Geochemistry, Geophysics, Geosystems* 5.5. DOI: 10.1029/2003GC000655.

Guo, Song et al. (2004b). "Re-evaluation of SO2 release of the 15 June 1991 Pinatubo eruption using ultraviolet and infrared satellite sensors". In: *Geochemistry, Geophysics, Geosystems* 5.4. DOI: 10.1029/2003GC000654.

Held, Isaac M. and Max J. Suarez (Oct. 1, 1994). "A Proposal for the Intercomparison of the Dynamical Cores of Atmospheric General Circulation Models". In: *Bulletin of the American Meteorological Society* 75.10, pp. 1825–1830. DOI: 10.1175/1520-0477(1994)075<1825:APFTIO>2.0.CO;2.

Lauritzen, P. H. et al. (May 4, 2015). "The terminator "toy" chemistry test: a simple tool to assess errors in transport schemes". In: *Geoscientific Model Development* 8.5, pp. 1299–1313. DOI: 10.5194/gmd-8-1299-2015.

McCormick, M. Patrick, Larry W. Thomason, and Charles R. Trepte (Feb. 1995). "Atmospheric effects of the Mt Pinatubo eruption". In: *Nature* 373.6513, pp. 399–404. DOI: 10.1038/373399a0.

Mills, Michael J. et al. (Mar. 16, 2016). "Global volcanic aerosol properties derived from emissions, 1990–2014, using CESM1(WACCM)". In: *Journal of Geophysical Research: Atmospheres* 121.5, pp. 2332–2348. DOI: 10.1002/2015JD024290.

Petty, Grant W. (2006). *A first course in atmospheric radiation.* 2nd ed. Madison, Wis: Sundog Pub. xii, 459 p.

Robock, Alan (May 2000). "Volcanic Eruptions and Climate". In: *Reviews of Geophysics*, p. 29.

– (Feb. 15, 2002). "The Climatic Aftermath". In: *Science* 295.5558, pp. 1242–1244. DOI: 10.1126/science.1069903.

Rosen, James M. (Oct. 1, 1971). "The Boiling Point of Stratospheric Aerosols". In: *Journal of Applied Meteorology and Climatology* 10.5, pp. 1044–1046. DOI: 10.1175/1520-0450(1971)010<1044:TBPOSA>2.0.CO;2.

Self, Stephen et al. (Jan. 1, 1993). "The Atmospheric Impact of the 1991 Mount Pinatubo Eruption". In.

Sheng, J.-X. et al. (Oct. 19, 2015). "A perturbed parameter model ensemble to investigate Mt. Pinatubo's 1991 initial sulfur mass emission". In: *Atmospheric Chemistry and Physics* 15.20, pp. 11501–11512. DOI: 10.5194/acp-15-11501-2015.

Stenchikov, Georgiy et al. (June 27, 1998). "Radiative forcing from the 1991 Mount Pinatubo volcanic eruption". In: *Journal of Geophysical Research* 1031, pp. 13837–13858. DOI: 10.1029/98JD00693.

Stenchikov, Georgiy et al. (2021). "How Does a Pinatubo-Size Volcanic Cloud Reach the Middle Stratosphere?" In: *Journal of Geophysical Research: Atmospheres* 126.10, e2020JD033829. DOI: 10.1029/2020JD033829.

Toohey, Matthew et al. (Nov. 11, 2016). "Easy Volcanic Aerosol (EVA v1.0): an idealized forcing generator for climate simulations". In: *Geoscientific Model Development* 9.11, pp. 4049–4070. DOI: 10.5194/gmd-9-4049-2016.

U.S. Standard Atmosphere, 1976 (Oct. 1, 1976). NOAA-S/T-76-1562.

Williamson, David, Jerry G. Olson, and Byron A. Boville (Apr. 1, 1998). "A Comparison of Semi-Lagrangian and Eulerian Tropical Climate Simulations". In: *Monthly Weather Review* 126.4, pp. 1001–1012. DOI: 10.1175/1520-0493(1998)126<1001:ACOSLA>2.0.CO;2.

Yue, G. K. et al. (1994). "Stratospheric aerosol acidity, density, and refractive index deduced from SAGE II and NMC temperature data". In: *Journal of Geophysical Research: Atmospheres* 99 (D2), pp. 3727–3738. DOI: 10.1029/93JD02989.